J Nanopart Res (2010) 12:1905–1911
DOI 10.1007/s11051-009-9753-4

RESEARCH PAPER

Growth of monodisperse nanocrystals of cerium oxide during synthesis and annealing

Swapankumar Ghosh · Damodaran Divya · Kottayilpadi C. Remani · Thadathil S. Sreeremya

Received: 2 April 2009 / Accepted: 1 September 2009 / Published online: 17 September 2009

Abstract Monodisperse cerium oxide nanocrystals have been successfully synthesised using simple ammonia precipitation technique from cerium(III) nitrate solution at different temperatures in the range 35–80 °C. The activation energy for growth of CeO_2 nanocrystals during the precipitation is calculated as 11.54 kJ/mol using Arrhenius plot. Average crystal diameter was obtained from XRD analysis, HR-TEM and light scattering (PCS). The analysis of size data from HR-TEM images and PCS clearly indicated the formation of highly crystalline CeO_2 particles in narrow size range. CeO_2 nanocrystals precipitated at 35 °C were further annealed at temperatures in the range 300–700 °C. The activation energy for crystal growth during annealing is also calculated and is close to the reported values. An effort is made to predict the mechanism of crystal growth during the precipitation and annealing.

S. Ghosh (✉) · D. Divya · K. C. Remani · T. S. Sreeremya
National Institute for Interdisciplinary Science and Technology (NIIST), Council of Scientific and Industrial Research (CSIR), Trivandrum 695 019, India
e-mail: swapankumar.ghosh2@mail.dcu.ie

Present Address:
K. C. Remani
Department of Chemistry, Sree Neelakanda Government Sanskrit College, Pattambi 679 306, India

Keywords Cerium dioxide · Monodisperse · Nanocrystal · Growth · Kinetics

Introduction

Materials of nanodimension have been attracting increasing interest worldwide for their unique chemical and physical properties (Corradi et al. 2006) compared to bulk due to the enhanced surface area to volume ratio (Kamruddin et al. 2004), quantum confinement and changes in the lattice parameter and symmetry. CeO_2 commonly called as ceria, is a refractory material possessing face-centred cubic fluorite-type crystal structure (Patil et al. 2002) which is stable from room temperature to its melting point (Kang et al. 2006). Over the last two decades cerium oxide based materials have been extensively studied and employed in various applications including oxygen storage capacitors (Mai et al. 2005), catalysts (Murugan and Ramaswamy 2007), UV blockers (Zhang et al. 2003), gas sensors (Lyons et al. 2002), solid oxide fuel cells (Murray et al. 1999) and in chemical mechanical polishing (Lee et al. 2002; Suphantharida and Osseo-Asare 2004). Numerous techniques have been proposed to synthesise nanosized CeO_2 particles with promising control of size and properties, such as hydrothermal (Mai et al. 2005), reverse micelles (Masui et al. 1997), sonochemical (Yin et al. 2002), pyrolysis (Oh and Kim

2007), homogeneous precipitation (Tsai 2004) etc. and solvothermal/hydrothermal treatments have been developed towards shape-controlled CeO_2 nanomaterials (Mai et al. 2005). Among different synthesis methods, the precipitation technique has attracted the most extensive attentions owing to the advantages of the simple process, easy scale-up and low cost (Chen and Chang 2005). This method involves the simultaneous occurrence of nucleation, growth, coarsening and agglomeration processes, which will dramatically affect the size, morphology and properties of the products (Cushing et al. 2004). Materials exhibit grain growth during heat treatment. Control over grain growth during annealing is a crucial aspect for the thermal stability of nanocrystaline solids (Tjong and Chen 2004). The large ratio of surface area to volume for nanoparticles provides a tremendous driving force for diffusion, especially at elevated temperatures.

Most of the previous reports were focussed on the effect of calcination temperature on growth of CeO_2 nanocrystallites (Li et al. 2002; Kang et al. 2006; Li et al. 2003; Hirano and Kato 1999, 2000; Zhang et al. 2004; Zawadzki 2008; Mokkelbost et al. 2004) synthesised through different techniques. Yang et al. (2005) derived the activation energy (E) for growth during calcination for CeO_2 nanocrystallite synthesised by microwave heating. Chen and Chang (2005) reported the particle growth as a function of reaction temperature in CeO_2. Although cerium oxide nanocrystals prepared by the precipitation technique have been extensively studied, less information is reported on its growth kinetics during annealing and no data are available regarding the kinetics during crystallisation. Similar activation energy was reported by Tang et al. (2003) in magnetite system. In the present study, we report the effect of reaction as well as annealing temperatures on the size of CeO_2 nanocrystals synthesised by ammonia precipitation. The particle size, shape, distribution and crystalline structure of resulting particles were also demonstrated and discussed.

Experimental procedure

Ceria (CeO_2) nanoparticles were synthesised by the reaction of $Ce(NO_3)_3{\cdot}6H_2O$ (AR grade, Indian Rare Earths Ltd., India) and 25% ammonia solution (AR grade, Qualigens Fine Chemicals, India). In a typical synthesis, 582 ml 0.05 M cerium nitrate solution was added to ~34 ml 25% ammonia in a 2 l beaker at a uniform rate in 1 min under vigorous mechanical stirring, such that the hydroxyl/Cerium ratio (OH/Ce) in solution was greater than 10:1. The reaction was carried out at 35 °C (room temperature). A purple coloured precipitate formed within minutes after the addition of cerium nitrate solution. The precipitate turned to yellow on stirring further ~20 min indicating the formation of cerium oxide crystals. The stirring was continued for 2 h. The precipitation was carried out at temperatures in the range 35–80 °C with a total stirring time of 2 h. The precipitate was collected by centrifugation and the excess alkali was washed off with deionised water and ethanol several times. The precipitate was then dried at 65 °C in air oven. The sample identification code and their synthesis conditions are provided in Table 1. The ceria sample (K1, Table 1) synthesised with 0.05 M Ce concentration at room temperature was further annealed at different temperatures in the range 300–700 °C with 1 h exposure time to study their crystal growth.

The phase composition of the solid products were determined from the Powder X-ray diffraction patterns using a Philips X'PERT PRO diffractometer using Cu Kα radiation ($\lambda = 1.5406$ Å) and HR-TEM analysis. The XRD data were collected on oven dried powders in the 2θ range 20–65° at a scanning rate 2° min^{-1} with a step size 0.02°. High resolution transmission electron microscopy (HR-TEM) technique was used to characterise the morphologies of the materials and to confirm particle size and crystal structure. HR-TEM data were obtained using a FEI Tecnai 30 G^2 S-Twin High resolution Transmission electron microscope equipped with a Gatan CCD camera and operated at 300 kV. For TEM analysis, specimen powders were dried at 100 °C and were

Table 1 Synthesis conditions and their identification code of different cerium oxide samples prepared by ammonia precipitation at different temperatures

Sample name	Ce concentration (M)	Temperature (°C)	Time (h)
K1	0.05	35	2
K2	0.05	50	2
K3	0.05	65	2
K4	0.05	80	2

dispersed in isopropanol by ultrasonication. A micro drop of the suspension was then placed on a 400 mesh copper grid coated with transparent carbon. The grid was then dried naturally in air. Size measurements for the cerium oxide nanocrystals were performed at 25 °C by static light scattering (also referred to as Photon Correlation Spectoscopy, PCS) on a Zetasizer 3000 HSA, (Malvern, Worcestershire, UK) using a detection angle of 90° and a 60 mW He–Ne laser operating at a wavelength of 633 nm. A small amount of powder was ground well, dispersed in water, stirred mechanically and ultrasonicated to get a stable suspension. Nitrogen adsorption isotherms on selected nanocrystalline CeO_2 samples were determined at liquid nitrogen temperature (77 K) using a Micromeritics Gemini 2360 surface area analyser. Powder samples were degassed at 200 °C for 2 h in flowing dry nitrogen gas prior to the adsorption studies. The specific surface area of the CeO_2 powders were calculated from the N_2 adsorption data using the Brunauer–Emmett–Teller (BET) technique.

Results and discussion

The XRD patterns of CeO_2 samples synthesised at temperatures 35 and 65 °C are shown in Fig. 1. The diffraction peaks displayed almost all the characteristic diffractions corresponding to the face-centred cubic CeO_2, matching with the JCPDS pattern (Powder Diffraction File No 34-394) and the peaks were indexed.

The crystallite size (D_{XRD}) of CeO_2 powders was calculated from the X-ray line broadening by applying full width half maximum (FWHM) of characteristic peak (111) to the Scherrer equation given in Eq. 1

$$D_{XRD} = 0.9\lambda/(\text{FWHM Cos}\theta) \quad (1)$$

where λ is the wavelength of incident X-ray, and θ is the diffraction angle for the (111) plane. The intensity ratio for (111) to (200) reflections and the calculated crystallite size of all the CeO_2 samples synthesised at different temperatures are plotted against precipitation temperature and are shown in Fig. 2.

It can be seen that intensity of (111)/(200) increases nonlinearly with an increase in reaction temperature. This is due to the predominant occurrence of (111) plane over the plane (200), at higher temperatures as was also suggested by Chen et al. (Chen and Chang 2005). However, the rate of increase slows down with

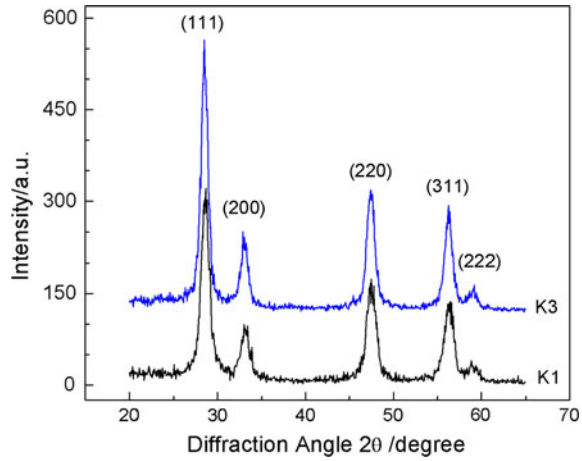

Fig. 1 X-ray diffraction patterns of K1 oven dried CeO_2 precipitated at 35 °C and K3 the same precipitated at 65 °C. The pattern for K3 is scaled for avoiding overlapping

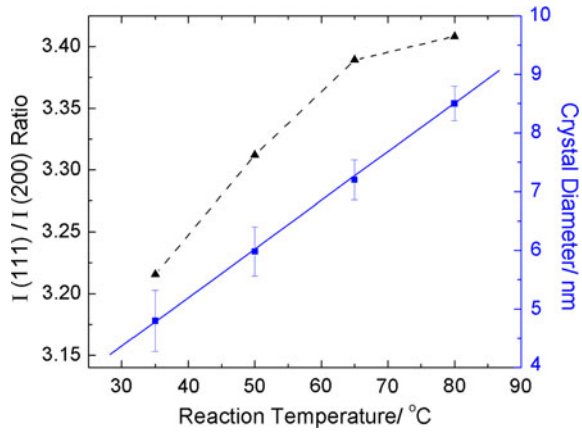

Fig. 2 Dependence of (*filled triangle*) intensity ratio (111)/(200) and (*filled square*) crystallite size of CeO_2 on reaction temperature during ammonia precipitation. The *blue solid line* is the linear fit to the size data

higher temperatures. The crystallite size is seen to increase linearly from 4.8 nm for K1 to 8.5 nm for K4 with increase in the temperature of reaction. The growth of crystals with the elevating reaction temperature proves that the growth rate of particles is predominant over the nucleation rate (Chen and Chang 2005).

Activation energy for crystal growth during synthesis

Activation energy for the growth of cerium oxide crystals during syntheses by ammonia precipitation at

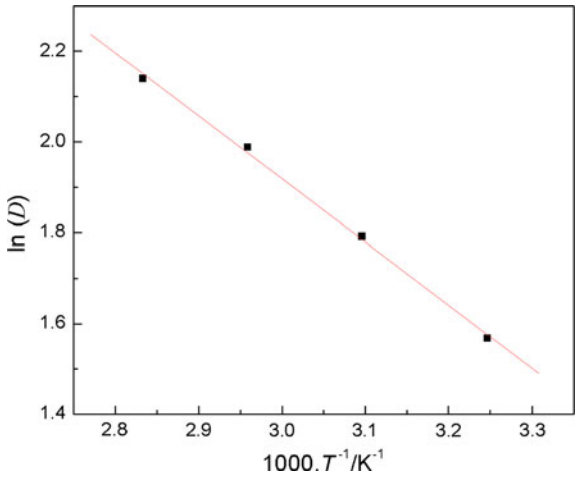

Fig. 3 Arrhenius plot of change in crystallite size as a function of reaction temperatures for ammonia precipitated CeO_2 samples with 0.05 M Ce precursor

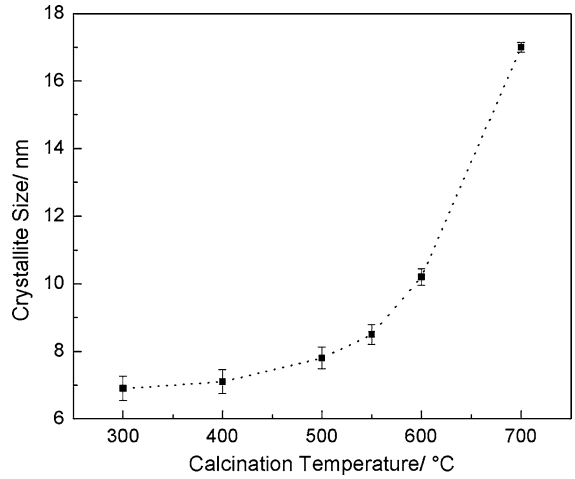

Fig. 4 Change in crystallite size with calcination temperature for samples prepared using ammonia and 0.05 M Ce precursor

different temperatures can be calculated using Arrhenius equation (Eq. 2)

$$D = \mathrm{C}\ \exp\ (-E/\mathrm{R}T) \quad (2)$$

where, D is the crystallite size of ceria, R the universal gas constant, T the reaction temperature in Kelvin, E is the activation energy and C is a constant which may depend on the initial value of crystal size (Kotera et al. 1963). The change in the crystallite size, ln(D) are plotted against the reaction temperature 1/T for the samples prepared at temperatures in the range 35–80 °C and is presented in Fig. 3.

Activation energy is calculated from the gradient of the linear regression to be 11.54 kJ/mol. This energy is responsible for initiating the complex process of nucleation and growth by diffusion as well as secondary growth by Ostwald ripening. The activation energy is relatively small as the nanocrystals have large surface area (not presented here). The growth process involves a dissolution–crystallisation mechanism (Hirano and Kato 1999) allowing a decrease of the free enthalpy of the system by reduction of the surface area. This process is under kinetically controlled regime during the initial steps of the precipitation.

Activation energy for crystal growth during calcination

Activation energy for growth of crystals during annealing was also estimated similarly for ammonia precipitated ceria sample (K1) using Arrhenius equation (Eq. 1). Small portions of the sample K1 were calcined at different temperatures in the range 300–700 °C. The furnace temperature was raised at a constant heating rate of 5 °C/min with a holding time (soak) of 1 h at peak temperature for all the samples. The crystallite size of the calcined powders was estimated using Scherrer formula (Eq. 1) and presented in Fig. 4. It is observed that the XRD patterns of powders obtained by annealing CeO_2 (K1) at 300–700 °C are all identical to that of CeO_2.

The XRD peak-width decreased (peak grew sharper) with increasing temperature and the average crystal size increased from 6.9 nm at 300 °C to 17.1 nm at 700 °C, indicating that the crystallinity of CeO_2 is enhanced by the calcination process. The exponential dependence with temperature indicates that crystallite coarsening is diffusion controlled (Li et al. 2002). Kotera et al. (1963) analysed crystal growth data on MgO, categorising the heating process into initial and later stages of calcination temperatures. Following his model, Arrhenius plot (ln D vs. 1/T) is shown in Fig. 5 for the temperature range 500–700 °C where the crystal growth is rapid.

The activation energy (E) for CeO_2 nanocrystal growth during calcination is calculated from the linear fit of the Arrhenius plot to be 24.85 kJ/mol. This value is close to ~20.5 kJ/mol reported by Yang et al. (2005) for microwave processed CeO_2 crystals of size ~6 nm. The higher value (E)

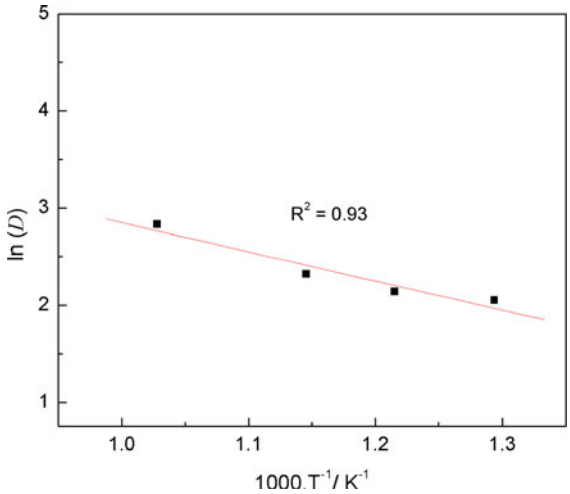

Fig. 5 Arrhenius plot of ln(D) against 1/T for ammonia precipitated sample K1 calcined at different temperatures

indicates that higher energy is needed for activation in the rapid growth stage of annealing.

The bright field HR-TEM images for K1 and K3 are presented in Fig. 6. The samples are highly crystalline as evidenced from the sharp SAED pattern (inset of Fig. 6a) and the pseudopolyhedral morphology can be viewed in the micrographs. The sample K1 is composed of particles in the size range 3–8 nm with a narrow distribution. The calculated average size on 100 particles for K1 is ~5.1 nm which is very close to crystal diameter of 4.8 nm calculated from XRD. As expected the average size of CeO_2 nanocrystals in sample K3 precipitated at 65 °C (shown in Fig. 6b) is higher ~7.2 nm (D_{XRD} 7.3 nm) with the sizes in the range 4–11 nm. The average particle size (D_{TEM}) and standard deviations (σ_{TEM}) were obtained by analysing the size data (obtained for more than 100 particles for all samples, from multiple TEM images). The standard deviation (σ_{TEM}) for sample K1 is 0.994.

The term σ_{TEM}/D_{TEM} (we denote by PDI_{TEM}) can be compared with the polydispersity index (PDI) in size data by light scattering techniques where it represents the narrowness of the size distribution (Stolarczyk et al. 2009). The PDI_{TEM} is estimated as 0.195 for K1 which is indicative of a monodisperse distribution. The BET surface area of K1 calculated from nitrogen adsorption isotherm is 148 m^2/g which also predicts an average particle size for K1 of ~5.5 nm (with an assumption that the particles are spherical and nonporous) which is very close to D_{TEM}.

The standard deviation (σ_{TEM}) for CeO_2 sample K3 is 1.65 with an average TEM size D_{TEM} as 7.2 nm which gives rise to PDI_{TEM} parameter as 0.229 which also indicates a fairly narrow (monodisperse) distribution of sizes in the sample. The particle size distribution from TEM images (log-normal fit) for K1 is presented in Fig. 7. The average particle sizes from TEM for CeO_2 samples K2 and K4 are 6 and 8.5 nm, respectively. The polydispersity indices (PDI_{TEM}) for K2 and K4 are 0.187 and 0.246, respectively (TEM images not presented here), which also supports the narrow size distribution of the fine CeO_2 particles.

The size measurement data from static light scattering for K1 in aqueous suspension are given in Fig. 8. Z-average diameters are the mean hydrodynamic diameter based upon the intensity of scattered light estimated from the analysis of the correlograms (using the General Purpose algorithm with Dispersion Technology Software v. 1.61, Malvern Instruments, UK).

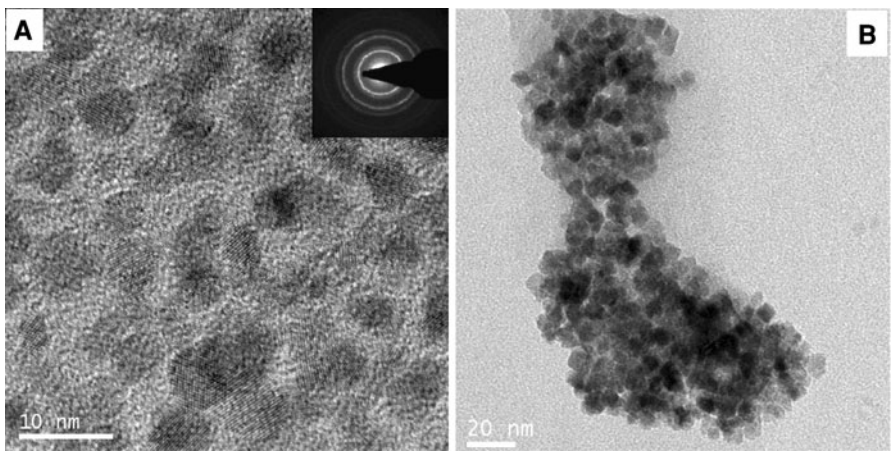

Fig. 6 HR-TEM images of cerium oxide nanoparticles precipitated at different temperatures. **a** K1 synthesised at 35 °C with D_{XRD} 4.8 nm. Average size of over 100 particles from multiple images is 5.1 nm with a standard deviation of 0.994, and **b** K3 precipitated at 65 °C with D_{TEM} 7.2 nm

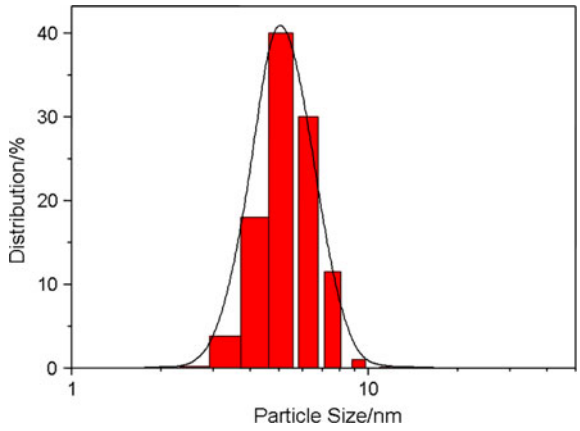

Fig. 7 Particle size distributions (histogram) as evaluated from TEM images of K1 CeO_2 yielding D_{TEM} as 5.1 ± 0.994 nm. The *solid line* represents the log-normal distribution of the CeO_2 particles

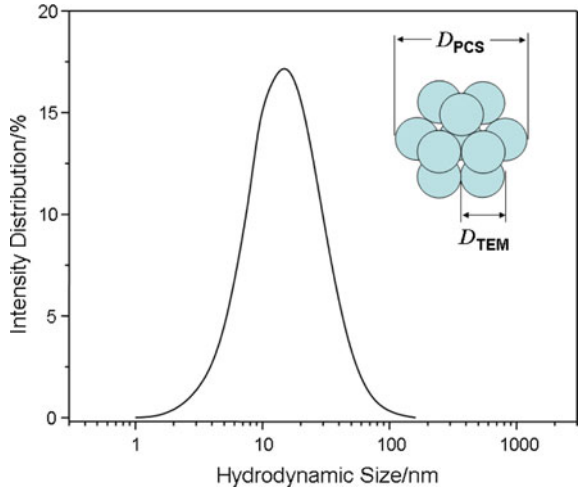

Fig. 8 Particle size distribution as measured by static light scattering (PCS) for ceria K1 dispersed in water with a D_{PCS} 16.2 nm and PDI 0.315. The inset is the schematic presentation of the one-shell cluster containing 13 primary particles. D_{PCS} is the hydrodynamic size of the cluster in suspension

The intensity distribution of Z-average diameter (D_{PCS}) for K1 is 16.2 nm with a PDI of 0.315. BET surface area, line broadening of XRD peaks as well as HR-TEM indicated an average nanocrystals size of ~5 nm for K1. The polydispersity index (PDI) estimates the width of the distribution. PDI value of 0.315 does not indicate a monodisperse suspension (Stolarczyk et al. 2009). This is due to the presence of particles of sizes in the range 5–30 nm with majority being ~16 nm. The D_{PCS} of ~16 nm could be due to one-shell clusters of a total of maximum 13 particles with average hydrodynamic diameter of ~3 × D_{TEM} which is 15.3 nm. The small nanoparticles of size ~5 nm have a tendency to cluster in water to reduce their high surface energy (due to high surface area to volume ratio) and hydrogen bonding in water. This confirms that the distribution of sizes determined from a XRD, HR-TEM, sp. surface area is indeed representative and the sample K1 is monodisperse.

Conclusions

Monodisperse ceria nanoparticles with size in the range 3–15 nm were synthesised by ammonia precipitation technique in the temperature range 35–80 °C. The XRD peak for CeO_2 crystals grew sharper with increasing temperature and the average crystal size increased on annealing from 6.9 nm at 300 °C to 17.1 nm at 700 °C, indicating that the crystallinity of CeO_2 is enhanced by the calcination process. The exponential dependence with temperature indicates that crystallite coarsening is diffusion controlled (Li et al. 2002). The activation energy for the growth of nanocrystallites during higher temperature of precipitation was estimated to be ~11.54 kJ/mol which is responsible for initiating the complex process of nucleation and growth by diffusion. Whereas the activation energy for growth of nanocrystals during calcination in the temperature range 500–700 °C was estimated as 24.85 kJ/mol. Small increase in the activation energy indicates that higher energy is required for activation in the rapid growth stage of annealing. The detailed analysis of TEM images and light scattering data has shown that all the samples were indeed monodisperse.

Acknowledgements This study was supported by the Indian Rare Earths Limited Technology Development Council (IRELTDC), DAE, India. We thank Department of Science and Technology (DST) and CSIR India for providing HR-TEM facility to NIIST. MMD (X-Ray), HR-TEM and SEM staff are kindly acknowledged for their assistance in obtaining XRD and electron microscopy data.

References

Chen HI, Chang HY (2005) Synthesis of nanocrystalline cerium oxide particles by the precipitation method. Ceram Int 31:795–802. doi:10.1016/j.ceramint.2004.09.006

Corradi AB, Bondioli F, Ferrari AM, Manfredini T (2006) Synthesis and characterization of nanosized ceria powders by microwave-hydrothermal method. Mater Res Bull 41:38–44. doi:10.1016/j.materresbull.2005.07.044

Cushing BL, Kolesnichenko VL, O'Connor CJ (2004) Recent advances in the liquid-phase syntheses of inorganic nanoparticles. Chem Rev 104:3893–3946. doi:10.1021/cr030027b

Hirano M, Inagaki M (2000) Preparation of monodispersed cerium(IV) oxide particles by thermal hydrolysis: influence of the presence of urea and Gd doping on their morphology and growth. J Mater Chem 10:473–477. doi:10.1039/a907510k

Hirano M, Kato E (1999) Hydrothermal synthesis of nanocrystalline cerium(IV) oxide powders. J Am Ceram Soc 82:786–788. doi:10.1111/j.1151-2916.1999.tb01838.x

Kamruddin M, Ajikumar PK, Nithya R, Tyagi AK, Raj B (2004) Synthesis of nanocrystalline ceria by thermal decomposition and soft-chemistry methods. Scr Mater 50:417–422. doi:10.1016/j.scriptamat.2003.11.010

Kang HS, Kang YC, Koo HY et al (2006) Nano-sized ceria particles prepared by spray pyrolysis using polymeric precursor solution. Mater Sci Eng B 127:99–104. doi:10.1016/j.mseb.2005.09.063

Kotera Y, Saito T, Terada M (1963) Crystal growth of magnesium oxide prepared by the thermal decomposition of magnesium hydroxide. Bull Chem Soc Jpn 36:195–199

Lee SH, Lu ZY, Babu SV, Matijevic E (2002) Chemical mechanical polishing of thermal oxide films using silica particles coated with ceria. J Mater Res 17:2744–2749. doi:10.1557/JMR.2002.0396

Li JG, Ikegami T, Wang YR, Mori T (2002) Reactive ceria nanopowders via carbonate precipitation. J Am Ceram Soc 85:2376–2378. doi:10.1111/j.1151-2916.2002.tb00465.x

Li YX, Zhou XZ, Wang Y, You XZ (2003) Preparation of nano-sized CeO_2 by mechanochemical reaction of cerium carbonate with sodium hydroxide. Mater Lett 58:245–249. doi:10.1016/S0167-577X(03)00454-3

Lyons DM, Ryan KM, Morris MA (2002) Preparation of ordered mesoporous ceria with enhanced thermal stability. J Mater Chem 12:1207–1212. doi:10.1039/b104677m

Mai HX, Sun LD, Zhang YW et al (2005) Shape-selective synthesis and oxygen storage behavior of ceria nanopolyhedra, nanorods, and nanocubes. J Phys Chem B 109:24380–24385. doi:10.1021/jp055584b

Masui T, Fujiwara K, Machida K et al (1997) Characterization of cerium(iv) oxide ultrafine particles prepared using reversed micelles. Chem Mater 9:2197–2204. doi:10.1021/cm970359v

Mokkelbost T, Kaus I, Grande T, Einarsrud MA (2004) Combustion synthesis and characterization of nanocrystalline CeO_2-based powders. Chem Mater 16:5489–5494. doi:10.1021/cm048583p

Murray EP, Tsai T, Barnett SA (1999) A direct-methane fuel cell with a ceria-based anode. Nature 400:649–651. doi:10.1038/23220

Murugan B, Ramaswamy AV (2007) Defect-site promoted surface reorganization in nanocrystalline ceria for the low-temperature activation of ethylbenzene. J Am Chem Soc 129:3062–3063. doi:10.1021/ja066834k

Oh H, Kim S (2007) Synthesis of ceria nanoparticles by flame electrospray pyrolysis. J Aerosol Sci 38:1185–1196. doi:10.1016/j.jaerosci.2007.09.007

Patil S, Kuiry SC, Seal S, Vanfleet R (2002) Synthesis of nanocrystalline ceria particles for high temperature oxidation resistant coating. J Nanopart Res 4:433–438. doi:10.1023/A:1021696107498

Stolarczyk JK, Ghosh S, Brougham DF (2009) Controlled growth of nanoparticle clusters through competitive stabilizer desorption. Angew Chem Int Ed 48:175–178. doi:10.1002/anie.200803895

Suphantharida P, Osseo-Asare K (2004) Cerium oxide slurries in CMP. Electrophoretic mobility and adsorption investigations of ceria/silicate interaction. J Electrochem Soc 151:G658–G662. doi:10.1149/1.1785793

Tang J, Myers M, Bosnick KA, Brus LE (2003) Magnetite Fe_3O_4 nanocrystals: spectroscopic observation of aqueous oxidation kinetics. J Phys Chem B 107:7501–7506. doi:10.1021/jp027048e

Tjong SC, Chen H (2004) Nanocrystalline materials and coatings. Mater Sci Eng R 45:1–88. doi:10.1016/j.mser.2004.07.001

Tsai MS (2004) Powder synthesis of nano grade cerium oxide via homogenous precipitation and its polishing performance. Mater Sci Eng B 110:132–134. doi:10.1016/j.mseb.2003.11.024

Yang HM, Huang CH, Tang AD, Zhang XC, Yang WG (2005) Microwave-assisted synthesis of ceria nanoparticles. Mater Res Bull 40:1690–1695. doi:10.1016/j.materresbull.2005.05.014

Yin L, Wang Y, Pang G, Koltypin Y, Gedanken A (2002) Sonochemical synthesis of cerium oxide nanoparticles-effect of additives and quantum size effect. J Colloid Interface Sci 246:78–84. doi:10.1006/jcis.2001.8047

Zawadzki M (2008) Preparation and characterization of ceria nanoparticles by microwave-assisted solvothermal process. J Alloys Compd 454:347–351. doi:10.1016/j.jallcom.2006.12.078

Zhang YW, Si R, Liao CS et al (2003) Facile alcohothermal synthesis, size-dependent ultraviolet absorption, and enhanced CO conversion activity of ceria nanocrystals. J Phys Chem B 107:10159–10167. doi:10.1021/jp034981o

Zhang F, Yang SP, Chen HM, Yu XB (2004) Preparation of discrete nanosize ceria powder. Ceram Int 30:997–1002. doi:10.1016/j.ceramint.2003.10.018